Molecular reorientation during dissociative multiphoton ionization

Peter Dietrich, Donna T. Strickland,* Michel Laberge,† and Paul B. Corkum
Steacie Institute for Molecular Sciences, National Research Council of Canada, Ottawa, Ontario, Canada K1A 0R6
(Received 18 September 1992)

The angular distribution of the ion fragments after multiphoton ionization of diatomic molecules shows a pronounced anisotropy. Fragments are detected mainly along the direction of the laser polarization, as is shown for iodine in this paper. We have performed a double-pulse experiment to clarify the underlying mechanism. It shows that the anisotropy cannot be explained in terms of a variation of the ionization rates with the angle between the electric field and the molecular axis. Instead, the anisotropy is caused by the deflection of the ion fragments in the strong field due to the molecular polarizability. Although the molecules are frozen in space on the time scale of the laser pulse, they gain enough angular momentum to affect the trajectories of the fragments. Classical trajectory calculations support this explanation.

PACS number(s): 33.80.Rv, 33.80.Gj, 33.80.Wz

I. INTRODUCTION

The study of multiphoton ionization of diatomic molecules at high intensities has revealed similarities to analogous experiments on atoms. For example, ionization in the long-wavelength limit (i.e., infrared at 10 μm) can be described by tunnel ionization models developed for atoms [1,2]. However, there are specific effects, like the polarizability or Stark shifts, which are much larger in molecules than in atoms. They have to be taken into account if we are to use atomic models to describe the ionization of molecular ions [3]. The polarizability is of particular interest because the interaction of a dipole with a strong field puts a torque on a molecule. For permanent dipole moments and constant fields, this torque has been used to align molecules [4–6].

The tendency of molecules to align in the presence of a strong laser field is well known in nonlinear optics [7]. Molecular alignment is responsible for the orientational-dependent optical Kerr effect, which has been studied extensively because of the insight it can give to molecular orientation in liquids [8,9]. The characteristic red shifts of the orientational optical Kerr effect have also been observed in ps experiments on continuum generation in molecular gases [10].

In this paper we will discuss a consequence of the orientational force in the dissociative ionization of diatomic molecules. A number of experiments [11–13] using linearly polarized light have indicated that the fragments are detected mainly along the direction of the laser polarization when ionizing a diatomic molecule into a repulsive state. However, there has been no quantitative explanation and even the qualitative nature has been unclear. We present here experimental and theoretical results to elucidate this phenomenon.

Highly charged molecular ions have no stable electronic state and must dissociate once they are formed. Thus the anisotropy of the fragment distribution can be explained in only two ways: either molecules perpendicular to the laser polarization are not ionized due an angular dependence of the ionization rates, or the fragments, though produced, are not detected.

To obtain experimental results which can be interpreted it is important that, classically speaking, the molecule does not rotate significantly during the ionization process. Therefore, we use ultrashort-laser pulses (30–80 fs) and a heavy molecule (I_2) which is frozen in space on the time scale of the laser pulse because the rotational period is $500/J$ ps. Here J is the angular-momentum quantum number. Furthermore, this allows us to detect fragments from dissociation of specific molecular states as each fragmentation channel yields a characteristic kinetic energy [13,14]. Thus we can measure the angular distributions for different fragmentation channels.

We will also show results from experiments that used two linearly polarized laser pulses polarized perpendicular to each other where the second pulse is delayed by 5 ps with respect to the first pulse. The results show that both polarizations interact essentially with all molecules. Therefore any angular dependence of the ionization rate is not important.

The polarizability is the key to understanding the angular distributions. It can be much larger in molecules than in atoms because, in parallel transitions, one moves electrons on the scale of the internuclear separation. This leads to large polarizabilities which, furthermore, increase quadratically with internuclear separation. Such a polarizable system experiences a large torque in a strong electric field if not aligned with the field. Although the molecules (or molecular ions) cannot move or rotate on the time scale of the laser pulse, it can gain enough angular momentum to deflect the trajectories of the fragments significantly. This leads to the observed angular distributions of the fragments.

The outline of the paper is as follows. In Sec. II we briefly describe the experimental setup. Section III contains the experimental results and a qualitative discussion. We show that we have to consider the dynamics of the fragmentation process in order to understand our data. In Sec. IV we discuss the dynamical behavior of the

polarizable molecule in a strong field. Section V gives the results of classical trajectory calculations of the fragmentation process. The last section summarizes the important points and gives an outlook on possible applications.

II. EXPERIMENTAL SETUP

The experimental setup consists of an ultrashort-laser pulse system and a time-of-flight mass spectrometer. A colliding pulse mode-locked dye laser [15] is used to produce 70-fs pulses at a wavelength of 625 nm. The pulses are amplified using a four-stage dye amplifier [16], pumped by a Q-switched Nd:YAG laser operating at a 10-Hz repetition rate. A single pass through a double-grating compressor is used at the output of the amplifier chain to compensate for the dispersion of the amplifier. After the compressor, the pulses have energies of 600 μJ and durations of 80 fs. A spatial filter which selects only the Airy disk of the transmitted radiation ensures a good spatial profile.

The laser pulses are focused inside a vacuum chamber by an on-axis $f/2$ parabolic mirror with a focal length of 50 mm. The aperture is limited to $f/20$ focusing in order to have a large number of molecules in the interaction region. To keep the intensity at the window of the chamber below the limit where nonlinearities modify the spatial properties of the beam, the energy is limited to 150 μJ. This gives a maximum intensity at the focus of about 10^{15} W cm^{-2}. The relative intensity of the laser pulses is determined by measuring the pulse energy. The absolute intensity scale is obtained by measuring Xe ionization and fitting the experimental results using the atomic tunneling model. Iodine is leaked into the chamber up to a maximum pressure of 4×10^{-5} mbar. Typically, the pressure is 10^{-6} mbar or below to avoid space-charge effects. The background pressure is 10^{-8} mbar.

For the double-pulse experiments, the laser pulses are split in a Michelson interferometer. A $\lambda/4$ wave plate in one arm of the interferometer rotates the linear polarization by 90°. To ensure that both pulses overlap inside the vacuum chamber, we use an undersized pinhole in a vacuum spatial filter. The pulses with polarization parallel to the time-of-flight axis are a factor of 2 weaker than the perpendicular pulses due to the two Brewster windows at the spatial filter. The combined pulses are then focused inside the chamber.

The ions are measured in a time-of-flight (TOF) mass spectrometer (see Fig. 1). In order to have the exploding ions situated symmetrically around the zero-kinetic-energy time, the accelerating and field-free regions of the TOF spectrometer have approximately equal distances of 30 and 32 mm, respectively. The focal spot is in the center of the accelerating plates. The accelerating voltage is typically 500–1000 V. For the data shown in this paper, we used a value of 600 V. The ions pass through a 2- and a 4-mm aperture at the output of the accelerating and field-free regions. At the end of the time-of-flight spectrometer, the ions are detected by a microchannel plate detector.

The time-of-flight spectra are recorded using one of two digital oscilloscopes with sampling rates of 400 MS/s

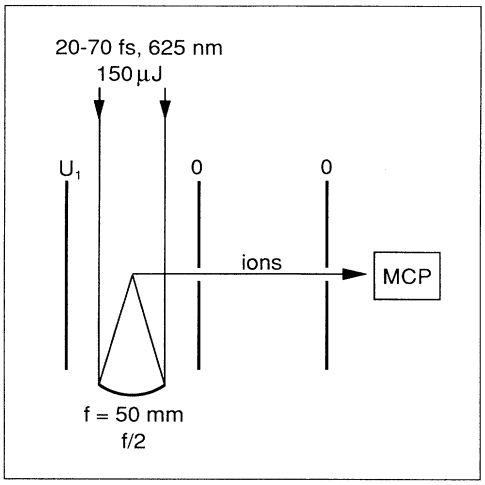

FIG. 1. Schematic of the time-of-flight mass spectrometer. The extraction plates are separated by 30 mm and kept on a voltage of 500–1000 V. The field-free drift length is 32 mm.

(Fig. 2) and 1 GS/s (Fig. 4). Ion yields are measured with boxcar integrators. The results shown here are corrected for the different size of the integration window. No attempt has been made to determine the sensitivity of the microchannel plate as a function of the energy (and charge) of the detected ions. Although the microchannel plate is operated at high gains near saturation, the detection efficiency may vary. Therefore, direct comparison of the yields for different ions should take this uncertainty into account. All results shown here are averaged over 1000 shots.

III. EXPERIMENTAL RESULTS

Figure 2 gives typical time-of-flight spectra for linearly polarized light at a peak intensity of about 10^{15} W cm^{-2}. The case of the polarization vector parallel to the time-of-flight axis [Fig. 2(a)] shows a rich structure which is discussed in detail in Ref. [14] (see also Ref. [13]). If the ions are produced with some initial kinetic energy, the time-of-flight spectrum will show pairs of peaks—one resulting from ions flying directly to the detector, the other from those ions which first fly in the opposite direction before being reversed by the extraction field. Each pair of peaks results from the fragmentation of ground (or excited) states of the different charge states of I_2^{n+} [13,14].

To assign a peak of the I^{k+} region to a fragmentation channel, we calculate the initial kinetic energy of the ions in this peak from the observed time of flight. For most peaks, the observed initial kinetic energy is close to the Coulomb energy between two positively charged ions I^{k+} and I^{l+} at the internuclear separation $R_e=0.2666$ nm. Thus we assign the respective peak to the fragmentation channel $I_2^{(k+l)+}\rightarrow I^{k+}+I^{l+}$. The lowest-kinetic-energy peaks of the I^+ and I^{2+} regions are assigned to fragmentation channels with one neutral fragment. Our assignment based on the kinetic energy has been confirmed by

recent correlation measurements where the correlations between the ion peaks have been observed [14,17]. The fact that a pair of peaks is a signature of the state produced in the ionization process allows us to measure the formation of these states in detail. For example, we can measure the angular distribution of the fragment ions for a given fragmentation channel (see below).

When using perpendicular polarization under otherwise unchanged conditions (i.e., the same intensity), the structure is much reduced, and the higher-charged ions disappear in the time-of-flight spectrum [Fig. 2(b)]. Only low-kinetic-energy I^+ and I^{2+} ions are observed in addition to the molecular ion I_2^+. This can be seen more quantitatively by measuring the angular distribution of the ion yields.

Figure 3 plots the number of fragment ions as a function of the angle between the laser polarization and the time-of-flight axis for the fragmentation channel $I_2^{3+} \rightarrow I^{2+} + I^+$. The linear laser polarization is rotated from $-90°$ to $+90°$ with respect to the time-of-flight axis using a $\lambda/2$ plate. The intensity of the laser pulses just exceeds that required to produce I_2^{3+}. The distribution is clearly peaked around the direction of the laser polarization.

Angular distributions have been measured for a number of different fragmentation channels, some of which are listed in Table I. With increasing degree of ionization, the anisotropy of the distributions becomes more pronounced. All distributions listed in Table I have been fitted using the empirical formula:

$$S(\theta) = a \cos^n \theta \ . \tag{1}$$

Both a and n are used as fitting parameters. The exponent n depends on the fragmentation channel. The values range from $n = 3$ at low-charge states to $n = 7$ for the highest-charge state investigated. The values for n seem to be independent of the peak intensity for a given fragmentation channel. This is consistent with the fact that a certain fragmentation channel is produced within a small intensity range. Changing the peak intensity only changes the volume of the shell in which this channel is produced. We note that both Eq. (1) and n are purely empirical and do not imply theoretical foundations. We also measured channels other than those listed in Table I. As expected, we observe no angular dependence for I_2^+ which is stable. The distribution for the channel $I_2^{2+} \rightarrow I^{2+} + I$ shows a much less pronounced anisotropy. The ion yields drop to about 50% at 90° relative to 0°.

We note that the measured distributions are broadened due to the geometry of the time-of-flight mass spectrometer which accepts ions with a finite transverse velocity with respect to the time-of-flight axis. The acceptance angle is determined by the extraction voltage and the size and the positions of the apertures along the drift path. For the given experimental conditions (extraction voltage 600 V, radius of the first aperture $R = 1$ mm), we estimate the acceptance angle $\Delta\theta$ assuming a pointlike ion source.

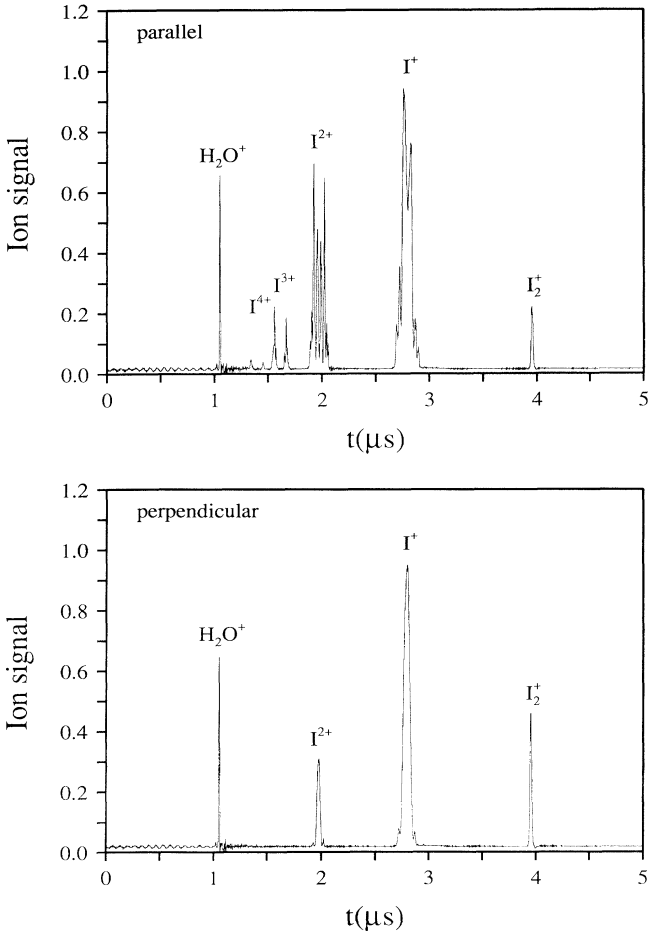

FIG. 2. Time-of-flight spectra for dissociative ionization of iodine. The intensity is $\sim 10^{15}$ W cm^{-2}. The laser pulse is linearly polarized with the electric-field vector pointing along the time-of-flight axis [parallel polarization (a)] and perpendicular to the time-of-flight axis [perpendicular polarization (b)].

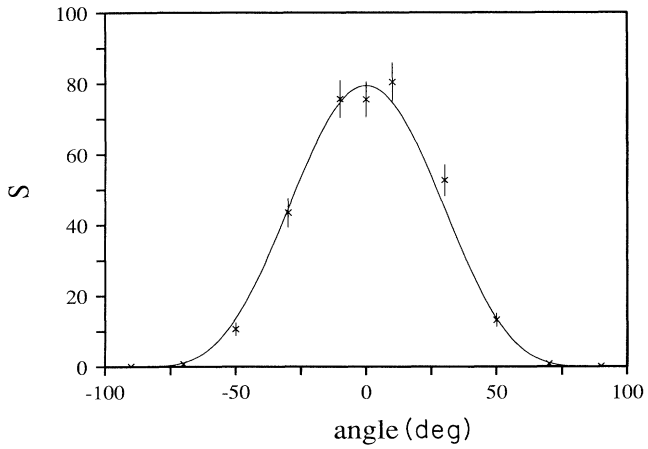

FIG. 3. Angular distribution for dissociative multiphoton ionization of I_2. Shown is the ion yield of the fragmentation channel $I_2^{3+} \rightarrow I^{2+} + I^+$ as a function of the angle between the laser polarization and the time-of-flight axis. The peak intensity is ca. 1.8×10^{14} W cm^{-2}, the acceptance angle is estimated to be 28°. The solid line is a fit with the empirical function $S(\theta) = a \cos^n \theta$, where $n = 4$ in this case.

TABLE I. List of fragmentation channels for which angular distributions have been measured and fitted using $S(\theta)=a\cos^n\theta$. The fragment which has been measured is listed first. Also given are the average peak intensity and the fitting parameter n with its standard deviation. The acceptance angle $\Delta\theta$ has been calculated assuming a pointlike ion source for an extraction voltage of 600 V and the geometry of our time-of-flight spectrometer. Only ions with an angle smaller than $\pm\Delta\theta$ will be detected.

Molecular ion	Ion fragments	I_0 (W cm^{-2})	n	$\Delta\theta$ (deg)
I_2^{2+}	$I^+ + I^+$	1.0×10^{14}	3.10±0.23	28
		1.5×10^{14}	3.00±0.24	28
I_2^{3+}	$I^{2+} + I^+$	1.8×10^{14}	4.28±0.25	28
I_2^{4+}	$I^{2+} + I^{2+}$	3.7×10^{14}	6.11±0.46	19
I_2^{4+}	$I^{3+} + I^+$	3.7×10^{14}	7.11±0.36	28

Only ion fragments with an angle smaller than $\pm\Delta\theta$ will be detected. The resulting values $\Delta\theta$ are listed in Table I and show that there is significant broadening of the observed distributions.

For highly charged molecular ions, there are only two possible explanations for the observed angular distributions. The first argues that molecules perpendicular to the laser field are not ionized or at least are ionized with a much smaller probability. The second assumes that the ionization is (more or less) independent of the angle between molecule and field, but the fragments are deflected towards the direction of the electric-field vector during dissociation. There are no other explanations possible because once a highly charged molecular ion is produced, it will dissociate. So either the molecular ion is not produced at 90° or the fragments are not observed.

Let us have a closer look at why the first explanation must be rejected. It assumes that molecules perpendicular to the polarization of the laser field are not ionized [11]. From the random distribution of molecular orientations in the gas phase, only molecules more or less parallel with the electric-field vector are ionized. Subsequently, the fragments come apart in the initial direction of the molecule. This explanation can be rejected for both theoretical and experimental reasons.

In Ref. [3] we discuss the weak angular dependence of the ionization rates. It is a result of the angular dependence of the Stark shifts and the induced dipole moments (see also Ref. [1]). Furthermore, the quadrupole moments will also suppress ionization for perpendicular molecules compared to parallel molecules. However, these effects do not change the ionization rates significantly. A typical change of 1.5 eV can easily be compensated by increasing the intensity by a factor of 2. Therefore, including these shifts into the calculation of the ionization yields would shift the calculated yields to higher intensities. But many experiments (including Fig. 1) are performed at intensities in the saturation regime. Even under these conditions, there are still hardly any ions observed at perpendicular polarization. This is not consistent with the molecular ionization model, which is otherwise quite successful. Thus, we conclude that an angular dependence of the ionization rates cannot explain the observed angular distributions.

To confirm the above conclusions experimentally, we have performed double-pulse experiments with parallel and perpendicular pulses (see Fig. 4). Both pulses have similar energy with a peak intensity of several 10^{14} W cm^{-4}, the perpendicular being more intense by a factor of 2. Using either of the two pulses (upper and lower trace in Fig. 4) we obtain the characteristic spectra as shown in Fig. 2. The middle trace shows the result when a perpendicular pulse precedes the parallel pulse by 5 ps. The perpendicular pulse strongly decreases the signals due to the parallel pulse. This holds also for a delay of 1 ps. This decrease means that molecules parallel to the second pulse are already ionized by the first pulse because the molecules cannot rotate on this time scale, thus proving that both polarizations interact with the same class of molecules.

We will show in the next two sections that the other explanation is valid. It argues that due to the anisotropy of the molecular polarizability, the fragments are

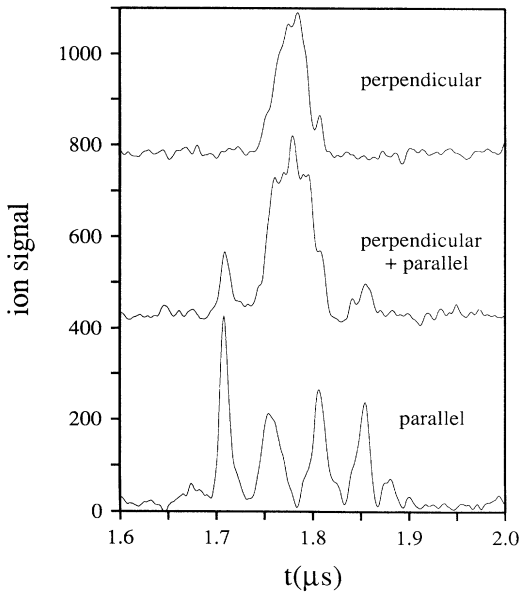

FIG. 4. Result of the double-pulse experiment with two pulses with linear polarization perpendicular to each other. Shown is the I^{2+} region of the time-of-flight spectra. Upper trace, perpendicular pulse only (polarization perpendicular to time-of-flight axis); middle trace, perpendicular pulse followed by a parallel pulse after 5 ps; bottom trace, parallel pulse only (polarization parallel with time-of-flight axis). The perpendicular pulse is a factor of 2 more intense than the parallel pulse.

deflected during dissociation. The interaction between the external field and the induced dipole moment results in a torque towards alignment with the field. This will lead to observed fragment distribution peaked around the direction of the field. Section IV discusses the influence of the molecular polarizability in a qualitative way. Section V contains numerical results from classical trajectory calculations.

IV. MOLECULAR POLARIZABILITY AND THE DYNAMICS OF THE FRAGMENT IONS

The polarizability of molecules is in general larger than that of atoms because of the larger size of the molecules. Quantum mechanically, a dipole moment is induced by coupling of states. The transition dipole moment and the energy gap determine the polarizability. Whereas the perpendicular polarizability is comparable to the polarizability of the atomic constituents because it results from transitions with the transition dipole moment perpendicular to the molecular axis, the parallel polarizability of diatomic molecules is often a factor of 2 larger than the perpendicular one because of the strength of the parallel transitions. Furthermore, the strongest parallel transition moments, which are due to charge-transfer or charge-resonance couplings, increase linearly with internuclear separation [18] leading to a quadratic increase of the parallel polarizability. Strictly speaking, this holds only for charge-resonance couplings as in odd charged molecular ions in their electronic ground state. For charge-transfer couplings, which are important for neutral molecules or even charge molecular ions in the electronic ground state, the linear increase of the transition moment near the equilibrium distance eventually turns over into an exponential decrease at large distances. Thus molecules, and especially molecular ions with odd charges, are highly polarizable systems.

When such a polarizable system is placed in a strong electric field, it will experience a strong torque if it is not aligned with the field. For a heavy molecule like I_2 and visible radiation, only the electrons can respond to the external field. The polarization force will thus give rise to an average force on the molecular constituents along the direction of the electric field. The angular component of this force leads to an increase of the angular momentum, whereas the radial component stretches the molecule. The increase of the angular momentum depends on the intensity and is, in the limit of low fields and heavy molecules, proportional to the fluence of the laser pulse. Large values of J can be reached. During fragmentation the angular momentum will rotate the molecule or the fragments towards the direction of the polarization. The deflection angle, i.e., the change of the molecular axis, depends on the initial angle between the field and the molecule, the electric-field amplitude, and the repulsive force between the two fragments. Calculations of the fragment trajectories will be discussed in the next section. Qualitatively, the fragment trajectories can end up aligned with the direction of the electric field, as observed experimentally.

V. CLASSICAL TRAJECTORY CALCULATIONS

We have performed classical trajectory calculations to obtain a better understanding of the influence of the molecular polarizability. In our model calculations, we include a number of properties of iodine but leave out many of the less known details of I_2^{n+}. It is important to include the polarizability of the neutral molecule because it will lead to angular momentum before ionization. Once the molecule is ionized to a repulsive state, it immediately starts dissociating. The initial angular momentum at the start of fragmentation (i.e., when I_2^{n+} is formed) is critical for the calculated angular distribution. For the same reason, it is also necessary to use pulses with a Gaussian temporal profile instead of pulses with constant intensity. A square pulse leads to earlier ionization and thus less initial angular momentum than a Gaussian pulse where the neutral molecule experiences a slowly increasing electric field. The neutral molecule is modeled by taking a ground-state potential curve ($X\,^1\Sigma_g^+$ from I_2) and an ionic state ($D\,^1\Sigma_u^+$ from I_2) coupled by charge transfer. The transition dipole moment $\mu_{12}=\sqrt{2}eR/2$ leads to a parallel polarizability $\alpha_\parallel=14.7$ Å^3 for low intensities in good agreement with the experimental value [19]. To take the perpendicular polarizability into account, we reduce the transition dipole moment μ_{12} by a factor of $\sqrt{2}$ to obtain the value $\gamma=7.2$ Å^3 for the anisotropic polarizability [19].

We concentrate on the dissociation dynamics of the first purely repulsive charge state I_2^{3+} decaying into $I^{2+}+I^+$. From the fragment-ion states, one can construct the two states coupled by charge resonance. We assume that the potential curve of the upper state is given by a simple Coulomb potential. The potential curve of the lower state is the same Coulomb potential but superimposed is the attractive potential of the isoelectronic molecule Te_2^+ [20]. In this way we approximately include the attractive forces between the two ions due to the overlap of the electron shells (see Ref. [21]). The gap between the two curves at the equilibrium distance of the neutral molecule is 3.4 eV, the binding energy of Te_2^+. The charge-resonance coupling leads to a transition dipole moment $\mu_{12}=eR/2$. The absolute energy of the two charged states are adjusted so that the ionization potential equals 26.5 eV, which is the value for the ionization of $I_2^{2+}\rightarrow I_2^{3+}$ assuming a Coulomb potential for the upper charge state. The energy of the lower state is derived from the estimated ionization potential of 16.4 eV for $I_2^+\rightarrow I_2^{2+}$ [22].

We neglect the intermediate charge states for several reasons. These intermediate states are not well known, but the polarizabilities for the different charge states (the main parameters in our approach) should not be very different (i.e., varying less than a factor of 3) from that of I_2. The most important contribution to the polarizability in all charge species results from charge-transfer or charge-resonance couplings with very similar transition moments. Furthermore, the dynamics of the molecule should be similar in the different states as long as the state has a bound potential (I_2^{3+} is the first purely repulsive state). Thus, our calculations treat a model problem,

not the exact I_2 molecule.

The classical dynamics on one potential-energy curve has been calculated by direct integration of the equation of motions. We start with the classical Hamilton function. For simplicity, we assume that the direction of the electric field is in the plane of rotation. Then the Hamilton function for the homonuclear molecular in the center-of-mass frame is given by

$$H(r,p_r,\theta,L,t)=p_r^2/2\mu+L^2/2I+V(r)+V_{\text{int}} . \quad (2)$$

The first term on the right-hand side is the radial kinetic energy with the reduced mass μ and the radial momentum p_r. The second term is the rotational energy with the angular momentum L and the moment of inertia $I=\mu r^2$, where r is the internuclear separation. $V(r)$ is the field-free potential of the state on which the dynamic is calculated. The last term results from the coupling of the two states and includes the effect of the external field on the molecule. We use the quasistatic quantum-mechanical expression where the polarizability results from coupling of electronic states. Coupling two states, one has [1]

$$V_{\text{int}}=-V_{12}\cdot\tan\beta , \quad (3)$$

where $V_{12}(t)=-\mu_{12}\mathcal{E}(t)\cos\theta$ with the transition moment μ_{12}, the time-dependent electric field $\mathcal{E}(t)$ and the angle θ between the molecule and the electric field. β is given by $\tan 2\beta=2V_{12}/\Delta E$, where ΔE is the energy gap between the two coupled states. Equation (3) gives as the low-intensity limit the classical energy of a polarizable system in an electric field $V_{\text{int}}=-\gamma\mathcal{E}^2\cos^2\theta/2$, where γ is the anisotropic polarizability.

From the Hamilton function, Eq. (2), one can easily derive the equation of motions which are integrated using the Bulirsch-Stoer method [23]. Most of the calculations are done by averaging over one optical cycle. This leads to elliptic integrals and is justified because the molecule does not move on the time scale of the laser period (2 fs).

The ionization rates are calculated from the atomic tunneling model [24] (without molecular shifts). To simulate the random nature of the ionization, several trajectories with the same initial conditions are calculated where the exact time of ionization depends on the ionization rate at the momentary intensity and a random number. The initial conditions used in the results presented here are those of a molecule at rest in the equilibrium configuration. Ten ps after the maximum of the laser pulse (with Gaussian profile and full width at half maximum of 70 fs), the molecular fragments have reached their final angles. All final angles of trajectories of dissociated molecules are collected and smoothed to give the calculated angular distribution.

Figure 5 shows the normalized angular distribution for a peak intensity $I_0=3\times10^{14}$ W cm^{-2}. This intensity gives population of I_2^{3+} without significant further ionization. The distribution is clearly peaked around 0°, which is the direction of the electric-field vector. The width is comparable to those measured. We do not expect perfect agreement, as our model neglects a number of details of the real I_2 problem and does not include the

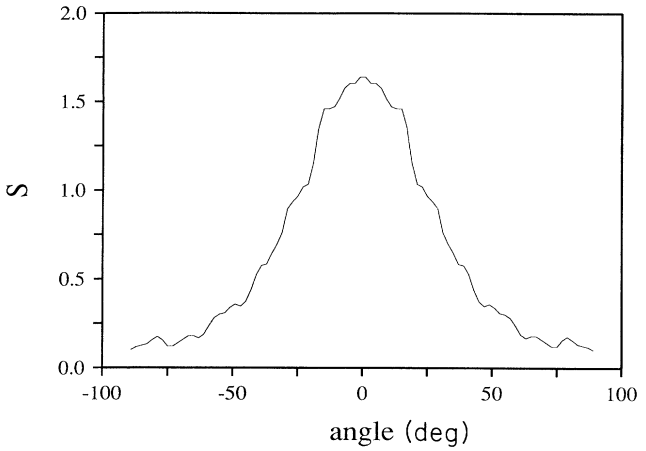

FIG. 5. Calculated angular distribution for dissociative multiphoton ionization for a simplified I_2 molecule. The calculation assumes a Gaussian temporal profile with a full width at half maximum of 70 fs and a peak intensity of 3×10^{14} W cm^{-2}. The spatial distribution has not been taken into account.

spatial intensity distribution. Nevertheless, the agreement is impressive. It clearly demonstrates that deflection of the ion fragments due to an increase of angular momentum can explain the observed angular distributions. With higher intensity, the torque on the molecule becomes larger, so that higher-charged molecules should show a more pronounced deflection, as indeed is observed.

An initial angular momentum of the molecule has little effect on the calculated angular distribution. Calculations with $J=\pm50$ (the most probable angular momentum at room temperature) yield identical distributions which are shifted by $\pm5°$. Superimposing them leads to the same distribution as $J=0$.

There are a number of possible improvements to our model. First, this problem should be addressed rigorously using a quantum-mechanical approach. There seems to be no simple theoretical approach available for treating a rotating molecule in a very strong time-dependent electric field [25]. Therefore we use a classical approach. Second, the charge-resonance energy levels have an energy separation on the same order as the photon energy. Single or multiphoton resonances can occur and clearly play a role in the dynamics of the molecular ion (not so much in the neutral molecule). Therefore our static polarizability must be replaced by the dynamic one, which again is not known in the high-intensity limit. The error induced by using the static instead of the dynamic polarizability is unlikely to change the angular distribution qualitatively, because the angular distribution depends mainly on the angular momentum absorbed when the internuclear distance is small and thus the laser frequency well below the resonance frequency. It will, however, have a strong effect on the kinetic energy of the ion fragments, which is increasing as long as the laser pulse is on.

Third, we have not included an angular dependence of the ionization rates. This might enhance the directionali-

ty because ionization is more likely for parallel than for perpendicular molecules. However, as stated above, this effect alone cannot explain the observations. Therefore we have concentrated on the influence of the polarizability. Note also that the present calculation does not include the spatial intensity distribution in the focal volume.

We thus think that the rather simple model shown here gives the basic explanation of the observed anisotropic angular distributions. Classically speaking, the polarizable molecule picks up angular momentum from the strong field leading to fragment trajectories with a large velocity component in the direction of the electric field.

VI. CONCLUSIONS

This paper presents a detailed study of the angular distributions observed in the dissociative multiphoton ionization of diatomic molecules. We show the importance of the molecular polarizability for the dynamics of the fragmentation process. The molecule and the molecular ion gain angular momentum due to the interaction with the strong electric field. This leads to the deflection of the fragment ions towards the direction of the electric field and thus explains the experimental observations. Classical trajectory calculations support this explanation.

Orientational processes such as those discussed in this paper are present in all high-field experiments and are particularly important when studying light molecules like H_2 or N_2 [11,12,26]. Interpretation of such long-pulse experiments will have to take the aligning forces into account.

We also note that not only the fragmentation process is affected. Because the neutral molecule gains angular momentum, it will eventually be aligned with the electric field. However, for a molecule like I_2, this will require ps at intensities of 10^{14} W cm^{-2}. Laser-induced angular trapping will be important for small molecules. It should be possible to trap the molecules in the potential well due to the polarizability. This should make it possible to conduct experiments with aligned molecules with a high degree of orientation.

This paper has also an important implication for nonlinear optics. The agreement between model and experiment suggests that Eq. (1) adequately describes the nonlinear response of the molecule. Plasmas consisting of molecular ions will be a very nonlinear medium which deserves further study.

ACKNOWLEDGMENTS

We thank D. Joines for continued technical support. P. Dietrich gratefully acknowledges financial support from the Deutsche Forschungsgemeinschaft, M. Laberge from the Centres of Excellence for Molecular and Interfacial Dynamics.

*Present address: Princeton University, Department of Chemistry, Princeton, NJ 08544.

†Present address: CREO Products, Inc., 370 Gilmore Way, Burnaby, BC, Canada V5G 4M1.

[1] P. Dietrich and P. B. Corkum, J. Chem. Phys. **97**, 3187 (1992).

[2] P. B. Corkum and P. Dietrich, Comments At. Mol. Phys. (to be published).

[3] P. Dietrich, D. T. Strickland, and P. B. Corkum (unpublished).

[4] H. J. Loesch and A. J. Remscheid, J. Chem. Phys. **93**, 4779 (1990).

[5] B. Friedrich and D. R. Herschbach, Nature (London) **353**, 412 (1991).

[6] B. Friedrich and D. R. Herschbach, Z. Phys. D **18**, 153 (1991).

[7] Y. R. Shen, *The Principles of Nonlinear Optics* (Wiley, New York, 1984), p. 297.

[8] D. McMorrow, W. T. Lotshaw, and G. A. Kenney-Wallace, IEEE J. Quantum Electron. **QE-24**, 443 (1988).

[9] G. L. Eesley, M. D. Levenson, and W. M. Tolles, IEEE J. Quantum Electron. **QE-14**, 45 (1978).

[10] P. B. Corkum (unpublished).

[11] L. J. Frasinski, K. Codling, P. Hatherly, J. Barr, I. N. Ross, and W. T. Toner, Phys. Rev. Lett. **58**, 2424 (1987).

[12] P. A. Hatherly, L. J. Frasinski, K. Codling, A. J. Langley, and W. Shaikh, J. Phys. B **23**, L291 (1990).

[13] D. T. Strickland, Y. Beaudoin, P. Dietrich, and P. B. Corkum, Phys. Rev. Lett. **68**, 2755 (1992).

[14] M. Laberge, P. Dietrich, and P. B. Corkum (unpublished).

[15] C. Rolland and P. B. Corkum, J. Opt. Soc. Am. B **5**, 641 (1988).

[16] C. Rolland and P. B. Corkum, Opt. Commun. **59**, 64 (1986).

[17] M. Laberge, P. Dietrich and P. B. Corkum, in *Ultrafast Phenomena VIII*, edited by L. J. Martin, A. Migus, G. A. Mourou, and A. Zewail (Springer-Verlag, Berlin, in press).

[18] R. S. Mulliken, J. Chem. Phys. **7**, 20 (1939).

[19] D. W. Callahan, A. Yokozeki, and J. S. Muenter, J. Chem. Phys. **72**, 4791 (1980).

[20] K. P. Huber and G. Herzberg, *Molecular Spectra and Molecular Structure. IV. Constants of Diatomic Molecules* (Van Nostrand Reinhold, New York, 1979).

[21] J. Senekowitsch and S. O'Neil, J. Chem. Phys. **95**, 1847 (1991).

[22] A. C. Hurley and V. W. Maslen, J. Chem. Phys. **34**, 1919 (1961).

[23] W. H. Press, B. P. Flannery, S. A. Teukolsky, and W. T. Vetterling, *Numerical Recipes* (Cambridge University, Cambridge, 1986).

[24] M. V. Ammosov, N. B. Delone, and V. P. Kraĭnov, Zh. Eksp. Teor. Fiz. **91**, 2008 (1986) [Sov. Phys.—JETP **64**, 1191 (1986)].

[25] J. F. McCann and A. D. Bandrauk, J. Chem. Phys. **96**, 903 (1992).

[26] A. Zavriyev, P. H. Bucksbaum, H. G. Muller, and D. W. Schumacher, Phys. Rev. A **42**, 5500 (1990).